Eur. Phys. J. B **8**, 453–461 (1999)

THE EUROPEAN PHYSICAL JOURNAL B

EDP Sciences

Interface polarons in a realistic heterojunction potential

S.L. Ban[a] and J.E. Hasbun[b]

Department of Physics, State University of West Georgia, Carrollton, Georgia 30118, USA

Received 17 September 1998

Abstract. The ground states of interface polarons in a realistic heterojunction potential are investigated by considering the bulk and the interface optical phonon influence. A self-consistent heterojunction potential is used and an LLP-like method is adopted to obtain the polaron effect. The numerical computation has been done for the $Zn_{1-x}Cd_xSe/ZnSe$ system to obtain the polaron ground state energy, self energy and effective mass parallel to the interface. A simplified coherent potential approximation is developed to obtain the parameters of the ternary mixed crystal and the energy band offset of the heterojunction. It is found that at small Cd concentration the bulk longitudinal optical phonons give the main contribution for lower areal electron densities, whereas the interface phonon contribution is dominant for higher areal electron densities. The interface polaron effect is weaker than the effect obtained by the three dimensional bulk phonon and by the two dimensional interface phonon models.

PACS. 73.40.Lq Other semiconductor-to-semiconductor contacts, $p-n$ junctions, and heterojunctions – 71.38.+i Polarons and electron-phonon interactions – 63.20.kr Phonon-electron and phonon-phonon interactions

1 Introduction

One of the consequences of the presence of the interface in a semiconductor heterojunction is that the conduction electrons are confined near it and these confined electrons have a two dimensional (2D) nature. The polaron effect associated with the electron-interface-phonon interaction needs to be considered. In general, there are enhanced polaron effects in lower dimensional systems. A 2D bulk phonon approximation was used to simplify the exact phonon modes in discussions of the 2D polaron ground state energy [1,2], the cyclotron resonance (CR) [3,4], and the 2D bound polarons problem [5]. The electron-phonon interaction of a realistic 2D system was overestimated in those works. In later work the interface polaron CR [6] and the electrophonon resonances [7] were discussed by only considering the influence of the three dimensional (3D) bulk longitudinal optical (LO) phonons. On the other hand, some authors discussed the polaron effects in heterojunctions [8,9] using a single effective interface-optical (IO) phonon branch to approximate the influence of IO phonons. However, this mechanism does not reflect the actual properties of IO phonon modes and needs to be improved. In the appearance of a detailed electron-phonon interaction mechanism in semicomductor heterostructures [10–14], it was found that the IO phonon mode frequencies depend on both LO and transverse optical (TO) bulk phonon frequencies. Thus the effects of the IO phonons as well as of the LO phonons were included in subsequent studies [15,16].

Taking both the bulk LO phonons and IO phonons into account and considering the interface as an infinite barrier, Degani and collaborators investigated interface polarons [15] in AlAs/GaAs heterojunctions, as well as interface bound polarons [16] in AlAs/GaAs and GaAs/GaSb systems under the influence of electric fields. Ban and coworkers obtained the 2D limit results of the IO phonon influence on the ground states [17] and CR [18] of the interface polarons in binary semiconductor heterojunctions. These authors [15–18] pointed out the significant effects of the actual IO phonons.

Recently, the exciton properties of $Zn_{1-x}Cd_xSe/ZnSe$ heterostructures have attracted much attention [19–21] since the blue-light emitter based on such II-VI compounds has been realized and the optoelectric devices within visible short-wave length spectrum region are potentially applicable. The optical phonons may play an important role on the binding energy of excitons in $Zn_{1-x}Cd_xSe/ZnSe$ quantum wells [20]. On the other hand, the basic understanding on the polaron effects in these heterostructures still lack and further investigation is needed.

In this paper, we discuss the influence of the bulk LO and IO phonons on the electronic ground states in semiconductor heterojunctions. For the quasi 2D electrons near the interface a realistic heterojunction potential is obtained using a self-consistent calculation [22,23] instead of an infinite barrier approximation [15]

[a] *Permanent address*: Department of Physics, Inner Mongolia University, Hohhot, China, 010021 P.R.

[b] e-mail: jhasbun@westga.edu

since the electron penetration into the barrier can not be neglected for heterojunctions with small ratio of the interface electron energy to the conduction band offset. For instance, for a Cd concentration region between $x = 0.05$ to 0.2 of a $Zn_{1-x}Cd_xSe/ZnSe$ heterojunction, the conduction band offset ranges between 50 meV and 200 meV [19] and our calculated interface polaron ground state energy ranges between 25 meV and 35 meV for electron density $N_s = 4 \times 10^{11}$ cm^{-2} and depletion charge density $N_d = 1 \times 10^{10}$ cm^{-2}. The motion of the conduction electrons in the direction parallel to the interface can be described by plane waves and the motion in the direction perpendicular to the interface becomes quantized due to the localization effect of the heterojunction potential. A one subband model is chosen here, without loss of generality, to describe the motion of the ground state electrons in the direction perpendicular to the interface. A modified LLP [15,24] unitary transformation is performed on the Hamiltonian of the electron-phonon interacting system to obtain the polaron self energy and effective mass parallel to the interface in a variational way. In order to perform the computation on the $Zn_{1-x}Cd_xSe/ZnSe$ heterojunction, a simplified coherent potential approximation (SCPA) [25–27] is developed here to obtain the bulk LO phonon frequency, the dielectric constants, the electron effective mass and the energy band gap of the ternary mixed crystal (TMC) $Zn_{1-x}Cd_xSe$. The numerical result is given for $Zn_{1-x}Cd_xSe/ZnSe$ heterojunction with Cd concentration $0.05 \leq x \leq 1$. For this situation, we demonstrate that the polaron effects are weakened even without considering the screening effects [28]. Our work is organized as follows: in Section 2, the Hamiltonian of the heterojunction and variational method based on unitary transformations deriving phonon contribution are discussed. In Section 3, the SCPA is introduced. The numerical result and discussion are given in Section 4. Finally, the conclusion is given in Section 5.

2 Hamiltonian and variational method

We consider a heterojunction consisting of two semiconductors with material 1 ($Zn_{1-x}Cd_xSe$) for $z > 0$ and material 2 (ZnSe) for $z < 0$. The interface of the heterojunction is chosen as the $x - y$ plane. For a finite heterojunction potential, conduction band electrons in material 1 (channel side) may penetrate into material 2 (barrier side). The Hamiltonian of an electron in a heterojunction potential interacting with bulk LO and IO phonons can be written as:

$$H = H_1 + H_2, \tag{1}$$

with

$$H_1 = -\frac{\hbar^2}{2}\frac{\partial}{\partial z}\frac{1}{m(z)}\frac{\partial}{\partial z} + V(z) \tag{2}$$

in which

$$m(z) = \begin{cases} m_{\perp 1} \text{ for } z > 0 \\ m_{\perp 2} \text{ for } z < 0 \end{cases}, \tag{3}$$

and

$$\begin{aligned} H_2 = &\frac{p_\parallel^2}{2m_{\parallel 1}}\theta(z) + \frac{p_\parallel^2}{2m_{\parallel 2}}\theta(-z) + \sum_{\mathbf{k}} \hbar\omega_{L1} a^\dagger_{\mathbf{k}1} a_{\mathbf{k}1}\theta(z) \\ &+ \sum_{\mathbf{k}} \hbar\omega_{L2} a^\dagger_{\mathbf{k}2} a_{\mathbf{k}2}\theta(-z) + \sum_{\mathbf{q},\sigma} \hbar\omega_\sigma b^\dagger_{\mathbf{q}\sigma} b_{\mathbf{q}\sigma} \\ &+ \sum_{\mathbf{k},\lambda}\left[\frac{B_\lambda \sin(k_z z)}{k} e^{-i\mathbf{k}_\parallel\cdot\boldsymbol{\rho}} a^\dagger_{\mathbf{k}\lambda} + h.c\right] \\ &+ \sum_{\mathbf{q},\sigma}\left[\frac{G_\sigma}{\sqrt{q}} e^{-i\mathbf{q}\cdot\boldsymbol{\rho}} e^{-q|z|} b^\dagger_{\mathbf{q}\sigma} + h.c\right]. \end{aligned} \tag{4}$$

In equation (2), $V(z)$ is the heterojunction potential which can be determined self-consistently. Here, $m_{\perp\lambda}$ and $m_{\parallel\lambda}$ are the band mass of the electron being in material $\lambda(\lambda = 1, 2)$ in the z-direction and in the x-y plane respectively. In equation (4), $\sigma = +(-)$ denotes the branch of IO phonon modes with higher(lower) frequency. The IO phonon frequencies can be obtained by solving [17] $\omega_\pm^2 = (b \pm \sqrt{b^2 - 4ac})/2a$, in which $a = \epsilon_{\infty 1} + \epsilon_{\infty 2}$, $b = \epsilon_{\infty 1}(\omega_{L1}^2 + \omega_{T2}^2) + \epsilon_{\infty 2}(\omega_{L2}^2 + \omega_{T1}^2)$, and $c = \epsilon_{\infty 1}\omega_{L1}^2\omega_{T2}^2 + \epsilon_{\infty 2}\omega_{L2}^2\omega_{T1}^2$. Here, $\omega_{L\lambda}$ ($\omega_{T\lambda}$) is the LO (TO) phonon frequency of the λ'th material. $\epsilon_{0\lambda}$ and $\epsilon_{\infty\lambda}$ are respectively the static and optical dielectric constants of the λ'th material. The interaction factors between an electron and bulk LO and IO phonons: B_λ and G_σ satisfy

$$B_\lambda = -i\left[\frac{4\pi e^2}{V}\hbar\omega_{L\lambda}\left(\frac{1}{\epsilon_{\infty\lambda}} - \frac{1}{\epsilon_{0\lambda}}\right)\right]^{1/2}\theta(\lambda, z) \tag{5}$$

with

$$\theta(\lambda, z) = \begin{cases} \theta(z) \text{ for } \lambda = 1 \\ \theta(-z) \text{ for } \lambda = 2 \end{cases}, \tag{6}$$

and

$$G_\sigma = i\left(\frac{1}{\delta_1^2 + \delta_2^2}\frac{2\pi\hbar e^2}{S\omega_\sigma}\right)^{1/2}, \tag{7}$$

where $\delta_\lambda = (\epsilon_{0\lambda} - \epsilon_{\infty\lambda})^{1/2}\omega_{T\lambda}/(\omega_{T\lambda}^2 - \omega_\sigma^2)$. In equations (4, 6), $\theta(\pm z)$ is a step function.

2.1 Displacement oscillator transformation with the coupling in the z direction

We adopt

$$\begin{aligned} U_1 = \exp\Bigg[\frac{i}{\hbar}\Bigg(&\mathbf{P}_\parallel - \hbar\sum_{\mathbf{k},\lambda}\mathbf{k}_\parallel a^\dagger_{\mathbf{k}\lambda} a_{\mathbf{k}\lambda}\theta(\lambda, z) \\ &-\hbar\sum_{\mathbf{q},\sigma}\mathbf{q} b^\dagger_{\mathbf{q}\sigma} b_{\mathbf{q}\sigma}\Bigg)\cdot\boldsymbol{\rho}\Bigg], \end{aligned} \tag{8}$$

and, following reference [15] but more appropriate for this work,

$$U_2 = \exp\left[\sum_{\mathbf{k},\lambda}\left(f_{k\lambda}e^{-ik_z z}a^{\dagger}_{\mathbf{k}\lambda} - f^{*}_{k\lambda}e^{ik_z z}a_{\mathbf{k}\lambda}\right)\theta(\lambda,z) + \sum_{\mathbf{q},\sigma}\left(g_{q\sigma}b^{\dagger}_{\mathbf{q}\sigma} - g^{*}_{q\sigma}b_{\mathbf{q}\sigma}\right)\right] \tag{9}$$

to perform two unitary transformations on Hamiltonian (1) and obtain the expectation value of energy:

$$E = \langle\psi \mid U_2^{-1}U_1^{-1}HU_1U_2 \mid \psi\rangle = E_1 + E_2, \tag{10}$$

where

$$\mid\psi\rangle = \mid\zeta(z)\rangle \mid 0\rangle = \mid\zeta(z)\rangle \prod_{\mathbf{k},\lambda,\mathbf{q},\sigma} \mid 0_{\mathbf{k}}\rangle \mid 0_{\mathbf{q}\sigma}\rangle. \tag{11}$$

In equation (9) $f_{k\lambda}$, $g_{q\sigma}$ and their complex conjugate are variational parameters. In equation (11), $\mid 0\rangle$ is the phonon vacuum state. The subband envelope function in the z direction for electrons in the ground state is $|\zeta(z)\rangle$. It is given by

$$\zeta(z) = \begin{cases} \zeta_A(z) = Bb^{1/2}(bz+\beta)e^{-bz/2} & \text{for } z > 0 \\ \zeta_B(z) = B'b'^{1/2}e^{b'z/2} & \text{for } z < 0, \end{cases} \tag{12}$$

where B, b, β, B' and b' are variational parameters [22,23] among which only b and b' are independent, while the rest are obtained through normalization and boundary conditions.

Minimizing equation (10) with respect to f and g, we obtain

$$E_1 = \langle\zeta(z) \mid -\frac{\hbar^2}{2}\frac{\partial}{\partial z}\frac{1}{m(z)}\frac{\partial}{\partial z} + V(z) \mid \zeta(z)\rangle, \tag{13}$$

and

$$E_2 = \frac{P_{\parallel}^2}{2m_{\parallel}^{*}} + \frac{\overline{p}_z^2}{2m_{\perp}}\frac{C_{LO}}{1+C_{LO}} + E_{LO} + E_I. \tag{14}$$

In equation (14), $\mathbf{P}_{\parallel}$ is the eigenvalue of the total momentum operator projection in the x-y plane. The polaron effective mass parallel to the plane is given by

$$m_{\parallel}^{*} = m_{\parallel}(1 + \Delta m_{LO} + \Delta m_I), \tag{15}$$

where the average electron band mass parallel to the x-y plane is defined as $m_{\parallel} = m_{\parallel 1}m_{\parallel 2}/(m_{\parallel 1}\overline{P}_2 + m_{\parallel 2}\overline{P}_1)$. Here $\overline{P}_1 = \int_0^{\infty} \mid \zeta_A(z) \mid^2 dz$ and $\overline{P}_2 = \int_{-\infty}^{0} \mid \zeta_B(z) \mid^2 dz$ are respectively the electron probabilities of being in material 1 and material 2. The contributions from LO and interface phonons to the effective mass are given by

$$\Delta m_{LO} = 2\frac{\hbar^2}{m_{\parallel}}\sum_{\mathbf{k}}\frac{\left|\phi_B(k_z)\right|^2 k_{\parallel}^2\cos^2(\theta)}{\left(\hbar\omega_{L1}\overline{P}_1 + \hbar\omega_{L2}\overline{P}_2 + \frac{\hbar^2k_{\parallel}^2}{2m_{\parallel}} + \frac{\hbar^2k_z^2}{2m_{\perp}}\right)^3}, \tag{16}$$

and

$$\Delta m_I = 2\frac{\hbar^2}{m_{\parallel}}\sum_{\mathbf{q},\sigma}\frac{\left|\phi_G(\sigma,q)\right|^2 q^2\cos^2(\theta)}{\left(\hbar\omega_{\sigma} + \frac{\hbar^2q^2}{2m_{\parallel}}\right)^3}, \tag{17}$$

where θ is the angle between $\mathbf{P}_{\parallel}$ and the wave vectors in the x-y plane. To simplify our calculation, we notice that $f_{k\lambda}$ is given in a form such as $f_{k\lambda} = a_{\lambda}/b_{\lambda}$. We assume without proof that $f_{k1} \sim f_{k2} = f_k$ (the probability of emitting or absorbing a bulk phonon of the electron in material 1 equals that in material 2) so that f_k is given by the proper form $f_k = \frac{a_1+a_2}{a_1+a_2}$. This is consistent with the straight simplification $\exp\left[\sum_{\mathbf{k},\lambda}\left(f_{k\lambda}e^{-ik_z z}a^{\dagger}_{\mathbf{k}\lambda} - f^{*}_{k\lambda}e^{ik_z z}a_{\mathbf{k}\lambda}\right)\theta(\lambda,z)\right] \rightarrow \exp\left[\sum_{\mathbf{k},\lambda}\left(f_k e^{-ik_z z}a^{\dagger}_{\mathbf{k}\lambda} - f^{*}_{k}e^{ik_z z}a_{\mathbf{k}\lambda}\right)\theta(\lambda,z)\right]$ in equation (9). Thus this is a reasonable approximation. The second term of equation (14) is the contribution from bulk LO phonons to the electron motion in the z direction. For the quantized energy level and the weak coupling between the electron and LO phonons, this term is not important. The numerically computed value of this term is less than 10^{-1} meV, which is negligible. In equation (14), we have used the definition $\overline{p}_z = \langle\zeta_A(z)|p_z|\zeta_A(z)\rangle m_{\perp}/m_{\perp 1} + \langle\zeta_B(z)|p_z|\zeta_B(z)\rangle m_{\perp}/m_{\perp 2}$, in which $m_{\perp} = m_{\perp 1}m_{\perp 2}/(m_{\perp 1}\overline{P}_2 + m_{\perp 2}\overline{P}_1)$, with the caveat that it is the magnitude of $\overline{p}_z$ that is used. C_{LO} reads

$$C_{LO} = 2\frac{\hbar^2}{m_{\perp}}\sum_{\mathbf{k}}\frac{\left|\phi_B(k_z)\right|^2 k_z^2}{\left(\hbar\omega_{L1}\overline{P}_1 + \hbar\omega_{L2}\overline{P}_2 + \frac{\hbar^2k_{\parallel}^2}{2m_{\parallel}} + \frac{\hbar^2k_z^2}{2m_{\perp}}\right)^3}. \tag{18}$$

The third and the forth term of equation (14) are the self energies of the polaron due to the contribution from LO and interface phonons respectively and are given by

$$E_{LO} = -\sum_{\mathbf{k}}\frac{\left|\phi_B(k_z)\right|^2}{\hbar\omega_{L1}\overline{P}_1 + \hbar\omega_{L2}\overline{P}_2 + \frac{\hbar^2k_{\parallel}^2}{2m_{\parallel}} + \frac{\hbar^2k_z^2}{2m_{\perp}}}, \tag{19}$$

and

$$E_I = -\sum_{\mathbf{q},\sigma}\frac{\left|\phi_G(\sigma,q)\right|^2}{\hbar\omega_{\sigma} + \frac{\hbar^2q^2}{2m_{\parallel}}}. \tag{20}$$

In the above equations, we have adopted the following notations:

$$\phi_B(k_z) = \sum_{\lambda}\langle\zeta(z) \mid \frac{B_{\lambda}\sin(k_z z)e^{ik_z z}}{k} \mid \zeta(z)\rangle, \tag{21}$$

and

$$\phi_G(\sigma,q) = \langle\zeta(z) \mid \frac{G_{\sigma}e^{-q|z|}}{\sqrt{q}} \mid \zeta(z)\rangle. \tag{22}$$

To determine the ground state energy, equation (10), we should solve equation (13) self-consistently to obtain

the variational parameters b and b' using the envelope function of equation (12). In equation (13), the heterojunction potential can be written as

$$V(z) = V_0\theta(-z) + V_s(z) + V_d(z), \tag{23}$$

in which V_0 is the potential barrier height, $V_s(z)$ the electron contribution to the potential and $V_d(z)$ the respective depletion charge contribution. The latter two terms can be obtained from

$$\frac{\partial}{\partial z}\epsilon_0(z)\frac{\partial}{\partial z}V_s(z) = -4\pi e^2 N_s \mid \zeta(z) \mid^2, \tag{24}$$

and

$$\frac{\partial}{\partial z}\epsilon_0(z)\frac{\partial}{\partial z}V_d(z) = -4\pi e^2 \left[N_A(z) - N_D(z)\right], \tag{25}$$

where N_s is the areal electron density, $N_A(z)$ and $N_D(z)$ the position dependent acceptor and donor concentrations. For the heterojunction system under consideration, E_1 has been analytically solved and is written simply as [23]:

$$E_1 = \langle T\rangle_{00} + \langle V_d\rangle_{00} + \langle V_s\rangle_{00} + \langle V_0\rangle_{00}, \tag{26}$$

where the subscript double zeros represent the matrix elements of equation (13). In equation (26),

$$\langle T\rangle_{00} = \frac{\hbar^2}{2}\left[(Bb)^2(1+\beta-\beta^2/2)/2m_{\perp 1} - (B'b')^2/4m_{\perp 2}\right], \tag{27}$$

$$\langle V_d\rangle_{00} = 4\pi e^2 N_d\left[-B^{'2}/b'\epsilon_{02} + B^2\left(6+4\beta+\beta^2\right)/b\epsilon_{01}\right)\Big], \tag{28}$$

$$\langle V_s\rangle_{00} = 4\pi e^2 N_s\Big[B^{'2}\left(1 - B^{'2}/2\right)/b'\epsilon_{02} + B^4\left(33+50\beta+34\beta^2+12\beta^3+2\beta^4\right)/4b\epsilon_{01}\Big], \tag{29}$$

and

$$\langle V_0\rangle_{00} = V_0 B^{'2}. \tag{30}$$

The polaronic effect, equation (14), on the electron states can be finally obtained by minimizing the total energy

$$E_T = E_1 + E_2 - \langle V_s\rangle_{00}/2 \tag{31}$$

with respect to the variational parameters b and b'.

2.2 Displacement oscillator transformation without the coupling in the z direction

We turn next to the second unitary transformation of equation (9) but without the phase factor [8,16]:

$$U_2 = \exp\left[\sum_{\mathbf{k},\lambda}\left(f_k a^\dagger_{\mathbf{k}\lambda} - f^*_k a_{\mathbf{k}\lambda}\right)\theta(\lambda,z) + \sum_{\mathbf{q},\sigma}\left(g_{q\sigma}b^\dagger_{\mathbf{q}\sigma} - g^*_{q\sigma}b_{\mathbf{q}\sigma}\right)\right] \tag{32}$$

and repeat the procedure described in Section 2.1. Equation (14) becomes

$$E_2 = \frac{P_\parallel^2}{2m^*_\parallel} + E_{LO} + E_I, \tag{33}$$

where the contribution from LO phonons (Eq. (19)) is given by

$$E_{LO} = -\sum_{\mathbf{k}}\frac{|\phi_{_B}(k_z)|^2}{\hbar\omega_{_{L1}}\overline{P}_1 + \hbar\omega_{_{L2}}\overline{P}_2 + \frac{\hbar^2k_\parallel^2}{2m_\parallel}}\cdot \tag{34}$$

Thus, the coupling between the electron and bulk phonons in the z direction has been neglected when one estimates the properties in the x-y plane.

The correction due to the bulk LO phonons to the polaron effective mass in equation (15) becomes

$$\Delta m_{_{LO}} = 2\frac{\hbar^2}{m_\parallel}\sum_{\mathbf{k}}\frac{|\phi_{_B}(k_z)|^2\,k_\parallel^2\cos^2(\theta)}{\left(\hbar\omega_{_{L1}}\overline{P}_1 + \hbar\omega_{_{L2}}\overline{P}_2 + \frac{\hbar^2k_\parallel^2}{2m_\parallel}\right)^3}\cdot \tag{35}$$

In equations (34, 35), we have used the notation

$$\phi_{_B}(k_z) = \sum_\lambda\langle\zeta(z)|\frac{B_\lambda\sin(k_z z)}{k}|\zeta(z)\rangle, \tag{36}$$

in contrast to equation (21). The rest of the quantities remain as given in the previous subsection.

3 Simplified coherent potential approximation (SCPA)

For a TMC $A_{1-x}B_x$ ($Zn_{1-x}Cd_xSe$) consisting of II-VI compounds A (ZnSe) and B (CdSe), the virtual crystal approximation (VCA) is not expected to be valid [25]. Let E_A (E_B) be the energy associated with a II-VI compound A (B). Then in the TMC system we make the ansatz that the corresponding energy is given by the solution of the CPA-like form [26,27]

$$\Sigma = E - (E_A - \Sigma)F(E_B - \Sigma), \tag{37}$$

where

$$E = xE_B + (1-x)E_A \tag{38}$$

is the VCA approximation energy. We take F in the real form

$$F = \frac{1}{Z - \Sigma}\cdot \tag{39}$$

If we further choose Z to have a null value, equation (37) can be solved analytically as

$$E_{TMC} = \frac{E_A E_B}{E_A + E_B - E}\cdot \tag{40}$$

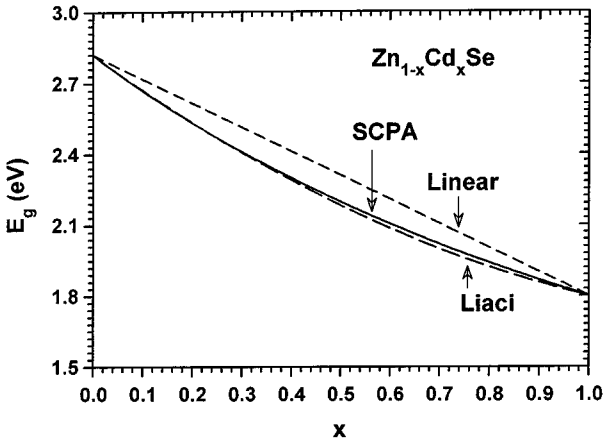

Fig. 1. The energy band gap E_g in units of eV of TMC $Zn_{1-x}Cd_xSe$ as a function of x. The solid line is the result calculated using SCPA. The long dashed line is the unstrained TMC result from Liaci [19]. The short dashed line is the linear interpolated or the VCA result.

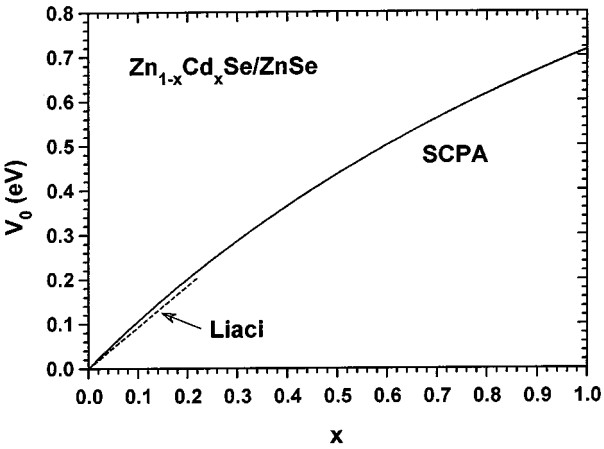

Fig. 2. The barrier potential V_0 of $Zn_{1-x}Cd_xSe/ZnSe$ heterojunction as a function of x. The dashed line is the result, which is believed to be valid for $x < 0.22$, with the strain effect from Liaci [19]. The solid line is the SCPA prediction for the full range of x.

For a slow moving electron in the TMC system, the effective mass approximation and the parabolic approximation for the energy band are still valid. Inserting the electron kinetic energy $E_k = \hbar^2k^2/2m$ into equation (40), we obtain the TMC electron band mass

$$m_{TMC} = xm_B + (1-x)m_A, \tag{41}$$

which is the same as the result obtained using the linear interpolation of reference [20] or the VCA.

Similarly, inserting the binding energy of a hydrogen-like impurity into equation (40), we derive the TMC dielectric constant

$$\epsilon_{TMC} = [((1-x)m_B\epsilon_A^2 + xm_A\epsilon_B^2)(x/m_A + (1-x)/m_B)]^{1/2}. \tag{42}$$

Adopting to the 70:30 rule [20] and using equation (40), we obtain the heterojunction barrier height

$$V_0 = 0.7 \times (E_{gA} - E_{gTMC}). \tag{43}$$

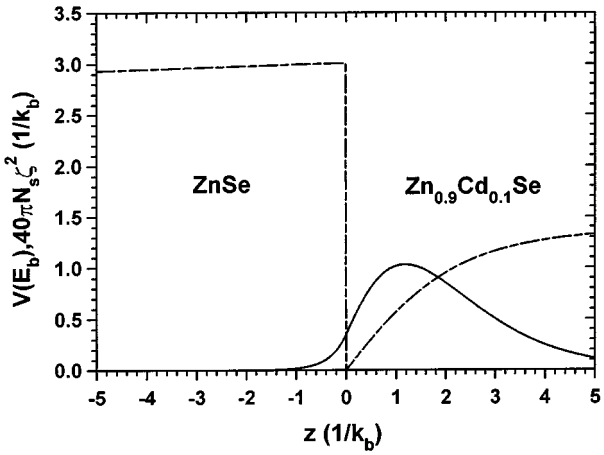

Fig. 3. Heterojunction potential (dashed line) in units of $E_b = me^4/2\hbar^2\epsilon_0^2 = 35.25$ meV and the electron (solid line) envelope function in units of $1/k_b (k_b = (2mE_b/\hbar^2)^{1/2} = 3.966 \times 10^6$ cm^{-1}) *versus* distance z in units of $1/k_b$ for $N_s = 4 \times 10^{11}$ cm^{-2}, $N_d = 1 \times 10^{10}$ cm^{-2} and $x = 0.1$.

4 Results and discussion

The numerical computation is performed on a $Zn_{1-x}Cd_xSe/ZnSe$ system in which x ranges from 0.05 to 1 so that our interface polaron model is expected to be properly treated. The parameters used in this work are given in Table 1. The SCPA is used to obtain the parameters of the TMC and the barrier height of the heterojunction. In the calculation, we take the band mass of the electron isotropic: $m_{\parallel} = m_{\perp}$.

The energy band gap of TMC $Zn_{1-x}Cd_xSe$ as a function of x is plotted in Figure 1. It can be seen that the SCPA result by equation (40) is in better agreement with the unstrained TMC result [19]. The barrier height is given in Figure 2. This figure contains the SCPA result for the full range of x. In contrast and in comparison we show the Liaci [19] result with strain effect which is only good for $x < 0.22$. In our work, we use the SCPA result.

For typical values of areal electron density $N_s = 4 \times 10^{11}$ cm^{-2}, areal depletion charge concentration $N_d = 1 \times 10^{10}$ cm^{-2}, and Cd concentration $x = 0.1$, the self-consistent results of the heterojunction potential and the electron envelope function *versus* z are given in Figure 3.

The polaron ground state energies $E_{gs,a}$ and $E_{gs,b}$ calculated using the result in Sections 2.1 and 2.2 as a function of N_s for $x = 0.1$ and $N_d = 1 \times 10^{10}$ cm^{-2} is given in Figure 4. There is only a negligible difference existing between $E_{gs,a}$ and $E_{gs,b}$ even though $E_{gs,b}$ is less than $E_{gs,b}$ in the range calculated.

As shown in equations (14, 33), the polaron self energy lowers the bare conduction electron energy in the $x - y$ direction. We compute this contribution for small

Table 1. Parameters used in computation.

Quantities	ZnSe(A)	CdSe(B)	$Zn_{1-x}Cd_xSe$[d]
E_g (eV)	2.82[a]	1.80[a]	$E_{gA}E_{gB}/(E_{gB}(1-x)+xE_{gA})$
$m(m_e)$	0.17[b]	0.13[b]	$xm_{_B}+(1-x)m_{_A}$
ϵ_0	8.1[b]	9.6[b]	$\left[\left((1-x)m_{_B}\epsilon_{0A}^2+xm_{_A}\epsilon_{0B}^2\right)(x/m_{_A}+(1-x)/m_{_B})\right]^{1/2}$
ϵ_∞	5.9[b]	5.98[b]	$\left[\left((1-x)m_{_B}\epsilon_{\infty A}^2+xm_{_A}\epsilon_{\infty B}^2\right)(x/m_{_A}+(1-x)/m_{_B})\right]^{1/2}$
$\hbar\omega_{_L}$(meV)	31[b]	27[b]	$\hbar\omega_{_{LA}}\omega_{_{LB}}/(\omega_{_{LB}}(1-x)+x\omega_{_{LA}})$
$\hbar\omega_{_T}$(meV)	25.5[c]	21.3[c]	$\hbar\omega_{_{TA}}\omega_{_{TB}}/(\omega_{_{TB}}(1-x)+x\omega_{_{TA}})$

[a] Reference [19].

[b] Reference [17].

[c] Evaluated by LST relation $\omega_{_T}=\omega_{_L}(\epsilon_\infty/\epsilon_0)^{1/2}$.

[d] SCPA.

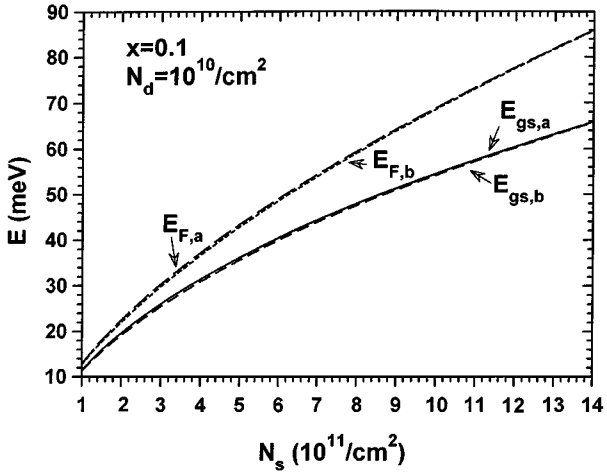

Fig. 4. The polaron ground state energies $E_{gs,a}$ and $E_{gs,b}$ in units of meV as functions of N_s in units of cm^{-2} for $x=0.1$ and $N_d=1\times10^{10}$ cm^{-2}. $E_{F,a}$ and $E_{F,b}$ are the Fermi energies. The subscripts a and b correspond to the results of Sections 2.1 and 2.2 respectively.

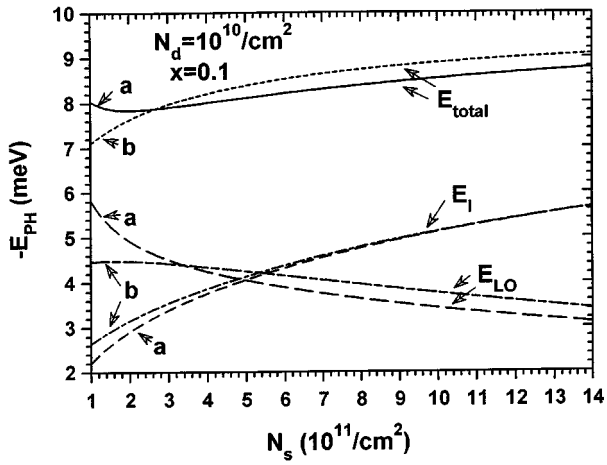

Fig. 5. The polaron self energies in units of meV as functions of N_s in units of cm^{-2} for $x=0.1$. $E_{total}=E_{LO}+E_I$. Curves labeled a and b correspond to the results of Sections 2.1 and 2.2 respectively.

$\mathbf{P}_\parallel$ case. Figure 5 gives the polaron self energies equations (19, 20, 34) *versus* N_s for a typical heterojunction with $x=0.1$ and $N_d=1\times10^{10}$ cm^{-2}. It is shown from the results of Section 2.1 that the contribution from LO phonons $-E_{LO}$ decreases whereas the contribution from IO phonons $-E_I$ increases with increasing N_s. This property can be easily understood since the energy band bending becomes more noticeable with increasing N_s. This effect forces the electrons to move towards the interface. For $x=0.1$, the electron coupling with IO phonons is weaker than the coupling with bulk LO phonons for small N_s. The opposite situation happens for large N_s. As a superposition, the total negative self energy first decreases then increases as N_s increases. In contrast with this, the result obtained in Section 2.2 shows that the contribution from LO phonons increases with N_s in the region of $N_s<1.7\times10^{11}$ cm^{-2}. This is physically unacceptable. The two curves of the total self energy obtained in Sections 2.1 and 2.2 intersect around $N_s=2.6\times10^{11}$ cm^{-2}. In the region of $N_s<2.6\times10^{11}$ cm^{-2}, equation (19) gives a more reasonable description of the contribution from the bulk LO phonons. When $N_s>2.6\times10^{11}$ cm^{-2}, the LO phonon contribution calculated from equation (34) also decreases as N_s increases, which is physically acceptable. Since equation (34) gives a lower total energy, it is expected to give more reasonable results when the electron is nearer the interface. On the other hand, the difference between the results obtained from equation (19) and from equation (34) is small within $N_s>1.7\times10^{11}$ cm^{-2}. It indicates that equation (19) also gives an acceptable result.

The average distance between an electron and the interface $\overline{z}=\langle\zeta_A(z)|z|\zeta_A(z)\rangle+\langle\zeta_B(z)|z|\zeta_B(z)\rangle$ as a function of N_s is given in Figure 6. It can be seen that as N_s increases the average distance $\overline{z}$ decreases rapidly at small N_s, then decreases slowly due to the comparatively stronger repulsion of the barrier at large N_s. In the region of small $\overline{z}$, the electron penetration into the barrier side is expected to give a direct influence on the polaron effect. The $\overline{z}$'s obtained using the results in Sections 2.1

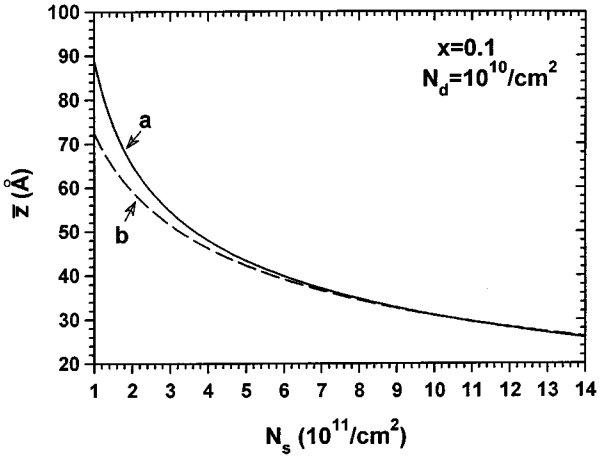

Fig. 6. The average distance between an electron and the interface $\overline{z}$ in units of cm as a function of N_s in units of cm^{-2} for $x = 0.1$. Curves labeled a and b are calculated by using the results of Sections 2.1 and 2.2 respectively.

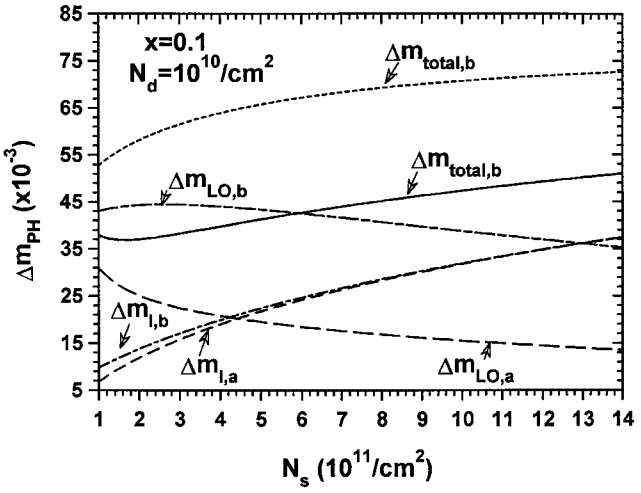

Fig. 7. The polaron effective mass corrections as functions of N_s in units of cm^{-2} for $x = 0.1$. $\Delta m_{total} = \Delta m_{LO} + \Delta m_I$. The subscripts a and b correspond to the results of Sections 2.1 and 2.2 respectively.

and 2.2 do not show an obvious difference with increasing N_s. This results in a close agreement between the IO phonon contributions obtained by the two methods.

The influence of LO phonons causes the electrons to move into the channel side, while the effect of the interface phonons is to attract them towards the interface. The LO phonons play a more important role in the competition for small N_s, whereas IO phonons are dominant for large N_s. With an increase in N_s, the fast decay of the contribution from LO phonons is responsible for total negative self energy decrease within a reasonable region. When $N_s > 1.7 \times 10^{11}$ cm^{-2}, the total negative self energy increases with N_s due to the slow decay of LO phonon influence and the comparatively fast increase of the IO phonon contribution.

Figure 7 shows the phonon contributions to the polaron effective mass as functions of N_s for $x = 0.1$ and $N_d > 1 \times 10^{10}$ cm^{-2}. The behavior of the contributions from bulk LO phonons, Δm_{LO}, and interface phonons, Δm_I, *versus* N_s is similar to that of the polaron self energies (Fig. 5). The results show that the contributions from LO phonons using equations (16, 35) have an obvious difference. This indicates that the polaron effective mass $m_{\|}$ is sensitive to the influence from the coupling in the z direction. This complex quasi 2D property needs to be investigated further both theoretically and experimentally.

For the given $N_s = 4 \times 10^{11}$ cm^{-2} and $N_d = 1 \times 10^{10}$ cm^{-2}, the polaron ground state energy, self energy and effective mass corrections *versus* x ($0.05 \leq x \leq 1$) are given in Figures 8, 9 and 10, respectively. That the result of Section 2.2 gives lower ground state energy for larger x indicates the model of Section 2.2 is more suitable for a system with 2D properties. The contributions from both the bulk LO and IO phonons are almost constant at large x because the electron position in the z direction is no longer sensitive to the Cd concentration when the barrier is high enough. Meanwhile, the influences from bulk

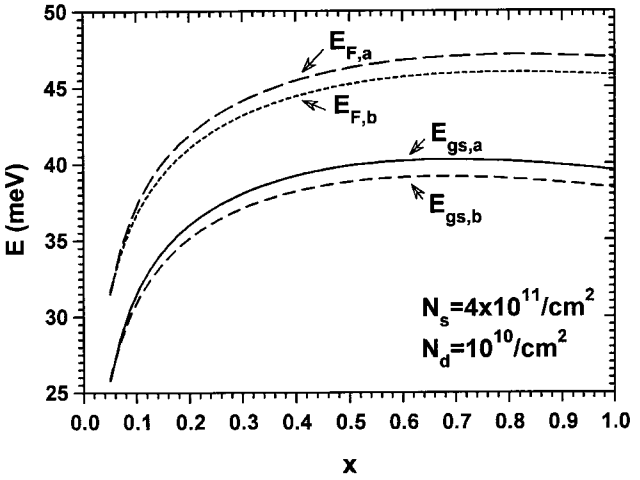

Fig. 8. The polaron ground state energies $E_{gs,a}$ and $E_{gs,b}$ in units of meV as functions of x for $N_s = 4 \times 10^{11}$ cm^{-2} and $N_d = 1 \times 10^{10}$ cm^{-2}. $E_{F,a}$ and $E_{F,b}$ are the Fermi energies. The subscripts a and b correspond to the results of Sections 2.1 and 2.2 respectively.

LO and IO phonons are comparable even though the LO phonons become dominant.

In Figures 9 and 10 the polaron self energies and effective masses obtained for two models are also plotted. One case is the 3D bulk LO phonon model, the other is the purely 2D IO phonon model. This shows that the present quasi 2D realistic model of Section 2.1 obtains weakened polaron effects.

In the limit of $b \sim b' \to \infty$ for the envelope function equation (12), the bulk LO phonon contributions $E_{LO} \to 0$ and $\Delta m_{LO} \to 0$ in equations (14, 33, 15). The polaron self energy has only one part from the IO phonon modes

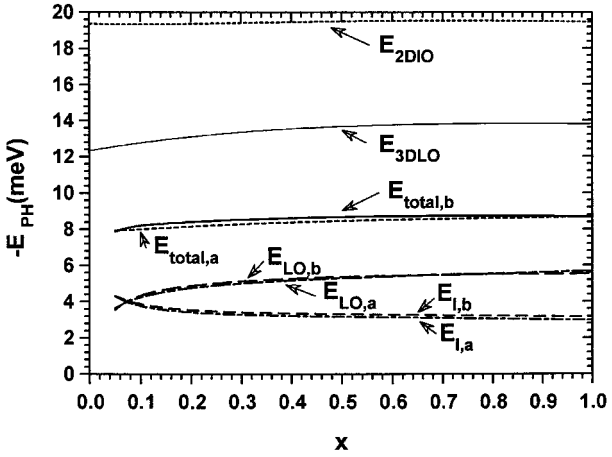

Fig. 9. The polaron self energies in units of meV as functions of x for $N_s = 4\times10^{11}$ cm^{-2} and $N_d = 1\times10^{10}$ cm^{-2}. $E_{total} = E_{LO} + E_I$. The subscripts a and b correspond to the results of Sections 2.1 and 2.2. E_{3DLO} and E_{2DIO} are the self energies obtained using the 3D bulk LO phonon model and the purely 2D IO phonon model respectively.

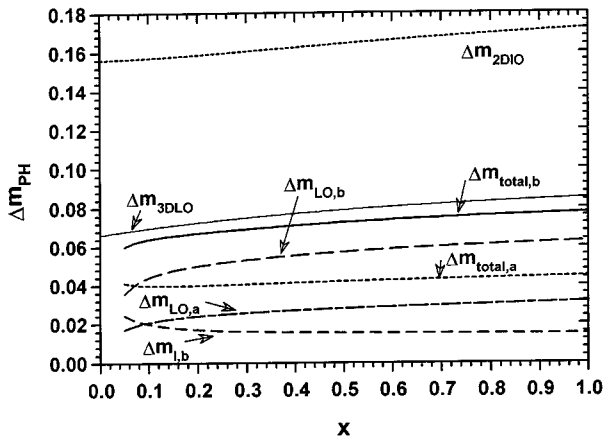

Fig. 10. The phonon contributions to polaron effective mass as functions of x for $N_s = 4\times10^{11}$ cm^{-2} and $N_d = 1\times10^{10}$ cm^{-2}. $\Delta m_{total} = \Delta m_{LO} + \Delta m_I$. The subscripts a and b correspond to the results of Sections 2.1 and 2.2. Δm_{3DLO} and Δm_{2DIO} are the effective masses obtained using the 3D bulk LO phonon model and the purely 2D IO phonon model respectively.

and reads

$$E_I = -\frac{\pi}{2}\sum_\sigma \hbar\omega_\sigma\alpha_\sigma, \tag{44}$$

where $\alpha_\sigma = 2e^2m_\parallel^{1/2}/\left[(\delta_1^2+\delta_2^2)\hbar^{3/2}\omega_\sigma^{5/2}\right]$ is the dimensionless electron-IO-phonon coupling constant. The polaron effective mass parallel to $x-y$ plane is given by

$$m_\parallel^* = m_\parallel(1+\frac{\pi}{8}\sum_\sigma\alpha_\sigma). \tag{45}$$

Equations (44, 45) are the expected 2D interface polaron result [17].

5 Conclusion

We have employed a self-consistent heterojunction potential to investigate the interface polaron effect contribution to the electronic ground state of a single heterostructure. An LLP-like variational method is used to obtain the polaron self energy and effective mass parallel to the interface. The numerical computation is performed for $Zn_{1-x}Cd_xSe/ZnSe$ heterojunction with the Cd concentration in the range of $0.05 \le x \le 1$. A simplified coherent potential approximation is developed to obtain the energy band gap, the dielectric constants and the band mass of the electron of the II-VI ternary mixed crystals. It is found that the interface polaron effects are weaker than the three dimension bulk polaron effects in the $Zn_{1-x}Cd_xSe$ material. While the bulk longitudinal optical phonons, for small Cd concentration, give the main contribution at low areal electron density, the interface phonon modes becomes dominant for high areal electron density. The interface phonons play a more important role than they do in III-V compound heterojunctions such as $GaAs/Al_xGa_{1-x}As$ [24].

S.L.B. was supported by the Fund for Excellent Young University Teachers of the State Educational Commission of China, the Chinese National Natural Science Foundation, and the China Scholarship Council. S.L.B. cordially thanks the hospitality of the State University of West Georgia during his visit. J.E.H. was supported by a Cottrell College Science Award of The Research Corporation.

References

1. Wu Xiaoguang, F.M. Peeters, J.T. Devreese, Phys. Rev. B **31**, 3420 (1985).
2. F.M. Peeters, J.T. Devreese, Phys. Rev. B **36**, 4442 (1987).
3. D.M. Larsen, Phys. Rev. B **33**, 799 (1986).
4. F.M. Peeters, Wu Xiaoguang, J.T. Devreese, Phys. Rev. B **34**, 1160 (1986).
5. S. Sil, A. Chatterjee, J. Phys.-Cond. **3**, 9401 (1991).
6. Wu Xiaoguang, F.M. Peeters, Phys. Rev. B **55**, 15438 (1997).
7. W. Xu, F.M. Peeters, J.T. Devreese, Phys. Rev. B **48**, 1562 (1993).
8. X.X. Liang, Solid State Commun. **55**, 215 (1985).
9. S.W. Gu, X.J. Kong, C.W. Wei, Phys. Rev. B **36**, 7971 (1987).
10. L. Wendler, R. Pechestedt, Phys. Status Solidi (b) **141**, 129 (1987).
11. L. Wendler, R. Haupt, Phys. Status Solidi (b) **143**, 487 (1987).
12. N. Mori, T. Ando, Phys. Rev. B **40**, 6175 (1989).
13. X.X. Liang, X. Wang, Phys. Rev. B **43**, 5155 (1991).
14. X.X. Liang, J. Phys.-Cond. **4**, 9769 (1992).

15. M.H. Degani, G.A. Farias, Phys. Rev. B **41**, 3572 (1990).
16. G.A. Farias, M.H. Degani, O. Hipólito, Phys. Rev. B **43**, 4113 (1991).
17. S.L. Ban, X.X. Liang, R.S. Zheng, Phys. Lett. A **192**, 110 (1994).
18. S.L. Ban, X.X. Liang, R.S. Zheng, Phys. Rev. B **51**, 2351 (1995).
19. F. Liaci, P. Bigenwald, O. Briot, B. Gil, N. Briot, T. Cloitre, R.L. Aulombard, Phys. Rev. B **51**, 4699 (1995).
20. R. Cingolani, P. Prete, D. Greco, P.V. Giugno, M. Lomascolo, R. Rinaldi, L. Calcagnile, L. Vanzetti, L. Sorba, A. Franciosi, Phys. Rev. B **51**, 5176 (1995).
21. A. Rajira, A. Abounadi, D. Coguillat, M. Averons, J. Calas, T. Cloitre, Solid State Commun. **105**, 229 (1998).
22. J.E. Hasbun, Phys. Rev. B **43**, 5147 (1991).
23. J.E. Hasbun, Phys. Rev. B **52**, 11989 (1995).
24. S.L. Ban, J.E. Hasbun, Bull. Am. Phys. Soc. **42**, 1789 (1997).
25. A.B. Chen, A. Sher, J. Vac. Sci. Technol. **21**, 138 (1982).
26. B. Velicky, S. Kirkpatrick, H. Ehrenreich, Phys. Rev. **175**, 747 (1968).
27. J.E. Hasbun, L.M. Roth, Phys. Rev. B **37**, 2829 (1987).
28. S. Das Sarma, B.A. Mason, Phys. Rev. B **31**, 5536 (1985).